SIAM J. APPL. MATH.
Vol. 69, No. 3, pp. 670–689

RECURSIVE DISPERSION RELATIONS IN ONE-DIMENSIONAL PERIODIC ELASTIC MEDIA*

ANI P. VELO†, GEORGE A. GAZONAS‡, ERWIN BRUDER†§, AND NANCY RODRIGUEZ†

Abstract. A frequency bandgap is a range of wave frequencies that are prohibited from passing through a medium. The dispersion relation, which links the frequency to the wave number, enables us to illustrate the bandgaps. In [E. H. Lee, "A survey of variational methods for elastic wave propagation analysis in composites with periodic structures," in Dynamics of Composite Materials, E. H. Lee, ed., ASME, New York, 1972, pp. 122–138] and [E. H. Lee and W. H. Yang, *SIAM J. Appl. Math.*, 25 (1973), pp. 492–499] the dispersion relation was studied theoretically for the one-dimensional periodic structure made of two materials arranged symmetrically with respect to the center of the cell. Their dispersion relation formulas can be similarly extended to a multilayered symmetric cell configuration, but not to a general (nonsymmetric) cell configuration. The general model was considered in [M. Shen and W. Cao, *J. Phys. D*, 33 (2000), pp. 1150–1154], where each unit cell of the periodic layered structure contains several sublayers of arbitrary lengths and materials. Using the transfer matrix method, the dispersion relation was successfully derived, involving very lengthy explicit formulas. In this paper, we generalize the work of Lee and Yang and develop recursive dispersion relation formulas for a general cell configuration. The recursive formulas are easy to implement and, through several numerical experiments, successfully corroborate the results of Shen and Cao.

Key words. dispersion relation, recursive formulas, wave propagation, Floquet theory, periodic layered media

AMS subject classifications. 35C05, 35R05

DOI. 10.1137/070692595

1. Introduction.

The existence of bandgaps in one-dimensional periodic elastic media appears to have been first established by Lord Rayleigh [17], and a good review of the early work on wave propagation in periodic elastic media can be found in Brillouin's classic text [2]; a more recent comprehensive review that outlines the development of the "band theory" for electrons, photons, and phonons can be found in Kushwaha [10]. A variety of technological applications has been suggested for phononic bandgap materials which include transducers, acoustic filters, or barriers for noise reduction, and even as a means for mitigating the effects of seismic surface waves. The study of phonons and phononic bandgaps associated with elastic wave propagation in periodic elastic media have also been used to study quantum field effects such as tunneling phenomena [24].

*Received by the editors May 21, 2007; accepted for publication (in revised form) July 17, 2008; published electronically December 5, 2008. This research effort was partially sponsored by the Faculty Research and Engineering Program (FREP), administered by the Battelle Memorial Institute in North Carolina for the U.S. Army Research Laboratory. This work was performed in part by an employee of the U.S. Government or under U.S. Government contract. The U.S. Government retains a nonexclusive, royalty-free license to publish or reproduce the published form of this contribution, or allow others to do so, for U.S. Government purposes. Copyright is owned by SIAM to the extent not limited by these rights.

http://www.siam.org/journals/siap/69-3/69259.html

†Department of Mathematics and Computer Science, University of San Diego, 5998 Alcalá Park, San Diego, CA 92110 (avelo@sandiego.edu).

‡U.S. Army Research Laboratory, Weapons and Materials Research Directorate, Aberdeen Proving Ground, MD 21005 (gazonas@arl.army.mil).

§The École Spéciale Militaire de Saint-Cyr, Coëtquidan, France.

Exact dispersion relations for harmonic waves in an infinite one-dimensional medium consisting of plane parallel alternating layers of two homogeneous isotropic elastic materials were derived in [20]. Their exact dispersion curves compare well with the "effective stiffness" theory they developed for the lowest vibrational modes over a wide range of wave numbers. Using a transfer matrix formalism and bypassing the use of Floquet theory, "pseudo-"stop bands and pass bands were computed in [3] for finite, periodically layered media. They showed that for a finite system containing at least ten cells, the characteristics of the second stop band compare well with that predicted in an infinite medium [11], [12] for a 2-2 composite consisting of ceramic and polymer constituents. This problem was further examined in [7], where it was shown that, in some instances, only one or two unit cells could be sufficient to depict the "frequency bandedness" seen in the infinite medium. Dispersion effects in finite periodic structures, which include viscous damping and the use of genetic algorithms for tailoring their frequency response characteristics, are also considered in [8].

Interestingly, the transfer matrix formalism has been successfully used for some time by geophysicists (e.g., [21], [5], [16], [1]), and for finite, layered Goupillaud-type (equal travel time) media [4], also known as the so-called communication matrix approach [19], [22], [9]. These works are not usually cited in prior work by the "bandgap" community, but are included here to emphasize their importance in providing insight and a framework for the analysis of dispersion effects in periodic elastic media.

Returning our attention once again to infinite media, [11] and [12] study the dispersion relation in an infinite strip of a periodically repeated cell with length or period a. According to their model, the cell is composed of two homogeneous elastic materials: the filler (f) and the matrix material (m). These materials are symmetrically arranged with respect to the center of the unit cell as shown in Figure 1.

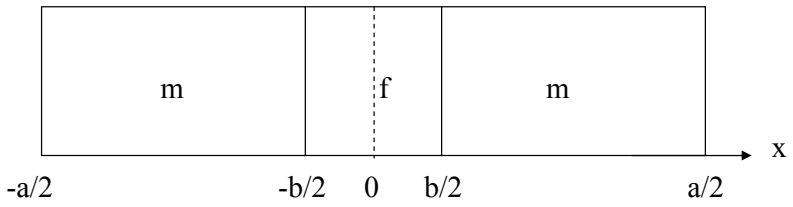

FIG. 1. *Symmetric unit cell made of two materials, used in* [11], [12].

The material density ρ and elastic modulus η are piecewise constant functions, taking constant values with subscripts f and m in the filler and matrix material regions, respectively. The density ρ and the elastic modulus η vary periodically along the strip with position x and period a,

$$\begin{cases} \rho(x+a) = \rho(x), \\ \eta(x+a) = \eta(x). \end{cases}$$

Figure 2 displays the density function within a single (unit) cell, assuming that $\rho_f \leq \rho_m$. Since the cell is periodically repeated in the infinite strip, the density graph shown in Figure 2 is also periodically repeated.

The general model was considered in [18], where each unit cell of the periodic layered structure contains several sublayers of arbitrary lengths and materials. They were

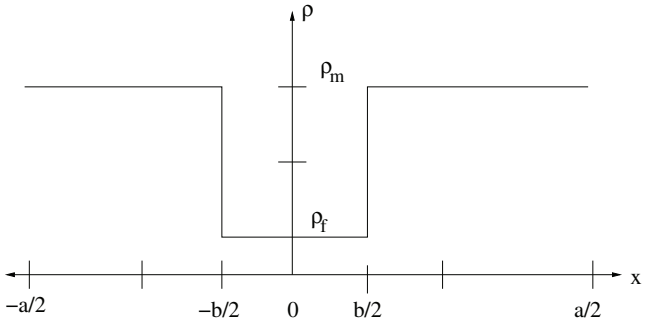

FIG. 2. *Density in a symmetric unit cell made of two materials.*

able to successfully derive the dispersion relation using the transfer matrix method, while involving very long explicit formulas.

In this paper, we generalize the work of [11], [12] and develop recursive dispersion relation formulas for a general cell configuration. The recursive formulas are easy to implement and, through several numerical experiments using Maple [15], successfully corroborate the results of [18].

Unlike the (two-material) symmetric cell configuration studied in [11], [12], the implicit dispersion relation for a general cell configuration appears to be more complex. The process of deriving an implicit recursive dispersion relation involves the construction of basic solutions in the unit cell, which provides more insight on how the properties of such solutions relate to the cell configuration. This is demonstrated through two approaches, which we identify as the central expansion approach and the quasi-symmetric limiting approach.

As shown in [11], [12], we begin with the wave equation with periodic coefficients η and ρ, described by

$$\frac{\partial[\eta\frac{\partial U}{\partial x}]}{\partial x} = \rho\frac{\partial^2 U}{\partial t^2}. \tag{1}$$

Using separation of variables, we assume that the displacement $U(x,t)$ can be expressed as

$$U(x,t) = u(x)\phi(t), \tag{2}$$

and (1) reduces to the second order ordinary differential equation with periodic coefficients,

$$\frac{d}{dx}\left[\eta\frac{du}{dx}\right] + \rho\omega^2 u = 0. \tag{3}$$

According to the Floquet theory, for a fixed ω, the solution $u(x)$ in (3) is of the form

$$u(x) = \upsilon(x)e^{iqx}, \tag{4}$$

where $\upsilon(x)$ is a periodic function with the same period a as the coefficients η and ρ. Due to the quasi-periodic recursive relation that follows from (4), we have

$$u(x+a) = u(x)e^{iqa},$$

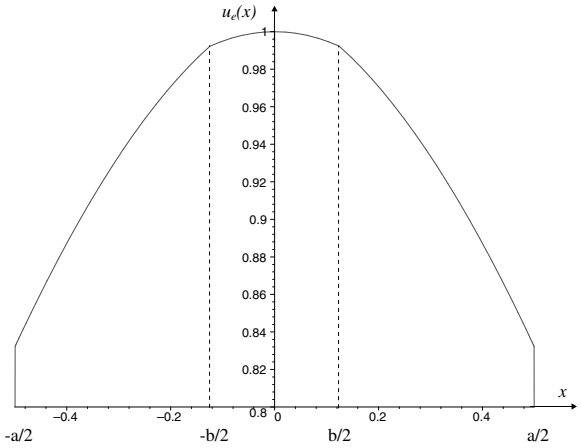

FIG. 3. *Even eigenfunction in a symmetric cell of two materials and three layers.*

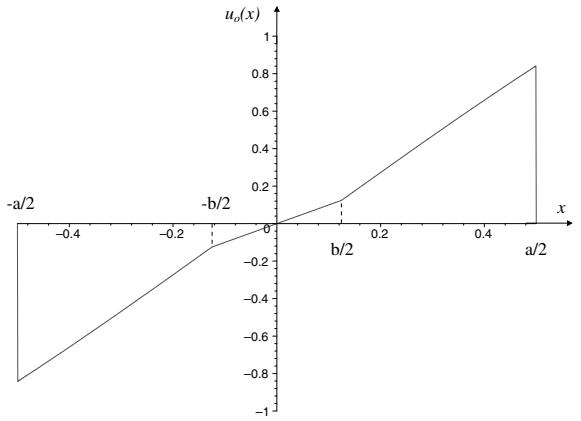

FIG. 4. *Odd eigenfunction in a symmetric cell of two materials and three layers.*

and the problem of finding the solution $u(x)$ along the strip is reduced to the single unit cell $-a/2 \leq x \leq a/2$, where the following quasi-periodic boundary conditions apply:

$$\begin{cases} u(a/2) = u(-a/2)e^{iqa}, \\ u'(a/2) = u'(-a/2)e^{iqa}. \end{cases} \tag{5}$$

The solution of (3) in the unit cell, subject to the boundary conditions (5), is then expressed as a linear combination of two eigenfunctions/linearly independent solutions of (3). For convenience, the two eigenfunctions are chosen to be even $u_e(x)$ and odd $u_o(x)$ functions along the symmetric cell studied in [11], [12]; see Figures 3 and 4. The solution of (3),

$$u(x) = u_e(x) + Cu_o(x), \tag{6}$$

satisfies the quasi-periodic boundary conditions (5) if

$$C = i\frac{u_e(a/2)}{u_o(a/2)}\tan\frac{qa}{2} \quad \text{and} \quad C = -i\frac{u_e'(a/2)}{u_o'(a/2)}\cot\frac{qa}{2}. \tag{7}$$

According to [11], [12], the compatibility of the two relations above results in the implicit form of the dispersion relation,

$$\boxed{\frac{u_e(a/2)}{u_o(a/2)}\tan\frac{qa}{2} = -\frac{u_e'(a/2)}{u_o'(a/2)}\cot\frac{qa}{2}.} \tag{8}$$

Further simplifications imply the following equivalent forms:

$$\tan^2\left(\frac{qa}{2}\right) = -\frac{u_e'(a/2)u_o(a/2)}{u_o'(a/2)u_e(a/2)}$$

or

$$\boxed{\cos(qa) = \frac{u_o'(a/2)u_e(a/2) + u_e'(a/2)u_o(a/2)}{u_o'(a/2)u_e(a/2) - u_e'(a/2)u_o(a/2)}.} \tag{9}$$

The dispersion relation is then obtained after the construction of the even and odd eigenfunctions $u_e(x)$ and $u_o(x)$ in the unit cell, and their substitution into (8) or (9). As discussed in [11], [12], due to (4), it is only necessary to consider the wave number q limited to the domain $0 \le q \le \pi/a$. The dispersion relation graph displays a banded frequency spectrum, comprising bands which transmit Floquet waves and no pass bands which do not.

2. Generalized form of the dispersion relation. In this section, we derive the dispersion relation for a general (unit) cell configuration, made of an arbitrary number of layers and materials. The steps involved are summarized below, and are generalizations of the work of [11], [12] discussed earlier. Through the rest of the paper, the interval of the unit cell with length a is $[-b, d]$. Here $0 < b, d < a$, and $b+d = a$. In the special case of a symmetric cell configuration seen before, $b = d = \frac{a}{2}$.

(i) The application of Floquet's theorem for (3), with ρ and η corresponding to the general (unit) cell configuration, yields two quasi-periodic conditions,

$$\begin{cases} u(x+a) = u(x)e^{iqa}, \\ u'(x+a) = u'(x)e^{iqa}. \end{cases}$$

Evaluating the conditions above at $x = -b$, we obtain the generalization of the boundary conditions (5),

$$\begin{cases} u(d) = u(-b)e^{iqa}, \\ u'(d) = u'(-b)e^{iqa}. \end{cases} \tag{10}$$

(ii) The solution $u = u(x)$ of (3) and (10) may be written in a general form similar to (6) as

$$u = C_1 u_1 + C_2 u_2. \tag{11}$$

Here $u_1 = u_1(x)$ and $u_2 = u_2(x)$ are two eigenfunctions/linearly independent solutions of (3), to be constructed later, while the constants C_1 and C_2 are unknown. For a symmetric cell configuration, such as the one studied in [11], [12], u_1 and u_2 become even and odd functions.

(iii) As a generalization of (7), after substituting (11) into the quasi-boundary conditions (10), we obtain a linear homogeneous system of equations for the unknowns C_1 and C_2,

$$\begin{cases} (u_1(d) - u_1(-b)e^{iqa})\,C_1 + (u_2(d) - u_2(-b)e^{iqa})\,C_2 = 0, \\ (u_1'(d) - u_1'(-b)e^{iqa})\,C_1 + (u_2'(d) - u_2'(-b)e^{iqa})\,C_2 = 0. \end{cases} \tag{12}$$

(iv) Seeking a nontrivial/nonzero solution, we set the determinant of the system (12) to zero, a condition which replaces the compatibility conditions used earlier in (7)–(8) by [11], [12]. This yields the $\omega = \omega(q)$ relation of the form

$$\boxed{\begin{aligned}&(u_1(d) - u_1(-b)e^{iqa})(u_2'(d) - u_2'(-b)e^{iqa}) \\ &= (u_1'(d) - u_1'(-b)e^{iqa})(u_2(d) - u_2(-b)e^{iqa}).\end{aligned}} \tag{13}$$

Equation (13) represents the dispersion relation for a general cell configuration in its implicit complex form.

(v) After a few manipulations of (13), using the property of the Wronskian $W(x)$ discussed below, we obtain the dispersion relation in its implicit real form. The Wronskian $W(x)$ of $u_1(x)$ and $u_2(x)$, two linearly independent solutions of the differential equation (3), is given by

$$W(x) = u_1(x)u_2'(x) - u_1'(x)u_2(x).$$

It directly follows from (3) that

$$\frac{d}{dx}[\eta(x)W(x)] = 0,$$

and therefore,

$$W(x) = \frac{C}{\eta(x)},$$

where C is a constant. Assuming that $\eta(-b) = \eta(d)$, one deduces that $W(-b) = W(d)$. Returning our attention to (13), after multiplying and reorganizing the terms, we obtain

$$W(d) - J(-b,d)e^{iqa} + W(-b)e^{i2qa} = 0, \tag{14}$$

where $J(-b,d) = u_1(-b)u_2'(d) + u_1(d)u_2'(-b) - u_1'(-b)u_2(d) - u_1'(d)u_2(-b)$.

Under the assumption that $\eta(-b) = \eta(d)$, one deduces that $W(-b) = W(d)$ and the relation (14) becomes

$$W(-b)[e^{iqa} + e^{-iqa}] = J(-b,d).$$

From here the dispersion relation is expressed in its implicit real form as

$$2\cos(qa) = \frac{J(-b,d)}{W(-b)},$$

or equivalently

$$\boxed{2\cos(qa) = \frac{u_1(-b)u_2'(d) + u_1(d)u_2'(-b) - u_1'(-b)u_2(d) - u_1'(d)u_2(-b)}{u_1(-b)u_2'(-b) - u_1'(-b)u_2(-b)}}. \tag{15}$$

Further simplifications follow if $u_1(x)$ and $u_2(x)$ are chosen to satisfy $u_1(-b) = u_2'(-b) = 1$ and $u_1'(-b) = u_2(-b) = 0$. Then $W(-b) = 1$ and the implicit dispersion relation,

$$2\cos(qa) = \frac{J(-b,d)}{W(-b)},$$

takes the form

$$2\cos(qa) = u_1(d) + u_2'(d).$$

Similar arguments can be found in [14].

A simplified form of (15) used to express the dispersion relation for the (two-material) symmetric cell configuration was derived in [11], [12] and given by (9). Indeed, when $b = d = \frac{a}{2}$, we obtain

$$2\cos(qa) = \frac{u_1(-\frac{a}{2})u_2'(\frac{a}{2}) + u_1(\frac{a}{2})u_2'(-\frac{a}{2}) - u_1'(-\frac{a}{2})u_2(\frac{a}{2}) - u_1'(\frac{a}{2})u_2(-\frac{a}{2})}{u_1(-\frac{a}{2})u_2'(-\frac{a}{2}) - u_1'(-\frac{a}{2})u_2(-\frac{a}{2})}. \tag{16}$$

Due to the symmetry of the cell configuration, u_1 and u_2 become even and odd functions, respectively. This means that

$$\begin{cases} u_1(\frac{a}{2}) = u_1(-\frac{a}{2}), \\ u_1'(\frac{a}{2}) = -u_1'(-\frac{a}{2}) \end{cases} \quad \text{and} \quad \begin{cases} u_2(\frac{a}{2}) = -u_2(-\frac{a}{2}), \\ u_2'(\frac{a}{2}) = u_2'(-\frac{a}{2}). \end{cases}$$

After substituting these relations into (16) and replacing $u_1 = u_e$ and $u_2 = u_o$, we obtain the dispersion relation (9), as seen before in [11], [12].

As a conclusion, relation (15) subject to the boundary requirement $\eta(-b) = \eta(d)$ represents the generalized form of the dispersion relation (9) derived in [11], [12]. This is also confirmed by our numerical experiments with the choice of the unit cell boxed in Figure 5, with border layers occupied by the same material, ensuring the same value for $\eta(x)$ and therefore the same value for $W(x)$ along the border layers.

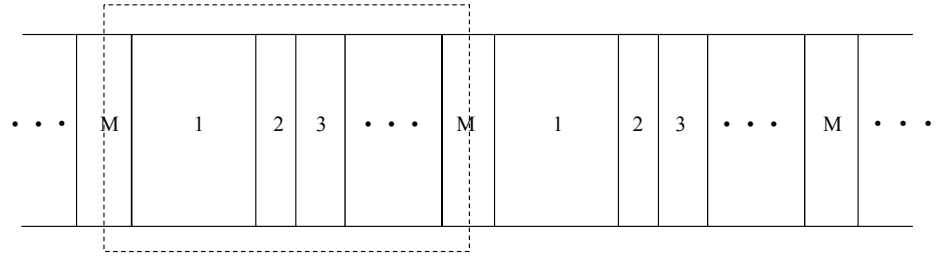

FIG. 5. *Unit cell selection in a periodic medium with a general cell configuration.*

3. Recursive formula of the dispersion relation using the central expansion approach. In order to develop the generalized dispersion relation (15), we need to find two eigenfunctions $u_1(x)$ and $u_2(x)$ of (3) in a unit cell of our choice. The unit cell of choice, used in the central expansion approach, is shown in the last diagram of Figure 6. This is obtained after shifting and renumbering the general cell

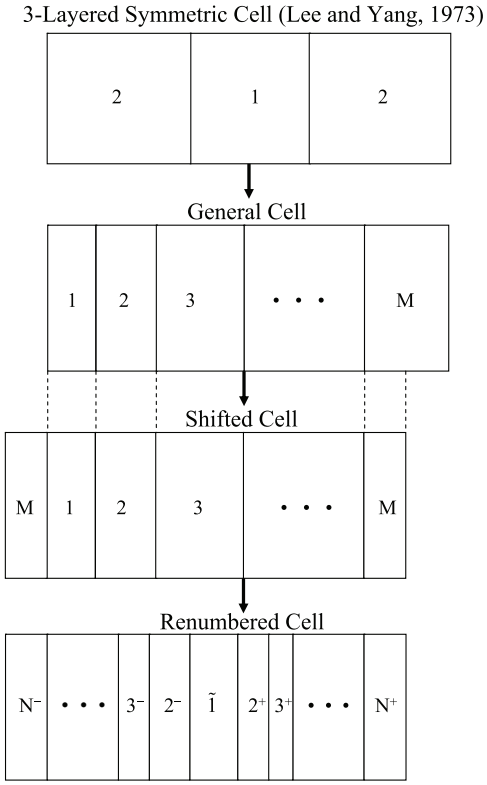

FIG. 6. *The stages of development of the central expansion approach for a given general cell configuration of M-layers. Here $N^+ = N^- = N$, where $N = \lceil \frac{M}{2} \rceil + 1$ or $N = \lceil \frac{M}{2} \rceil$.*

of M-layers. The purpose of the shifting is to have the border layers made of the same material to ensure that $\eta(-b) = \eta(d)$, which implies that $W(-b) = W(d)$ and therefore (15) holds. The purpose of the renumbering is to create a central layer in the cell similar to the three-layered symmetric cell configuration previously studied in [11], [12]. In the renumbered scheme, $N = \lceil \frac{M}{2} \rceil + 1$, unless the cell already has an odd number of layers M and the border layers are made of the same material, in which case $N = \lceil \frac{M}{2} \rceil$. The $(-)$ and $(+)$ superscripts on the renumbered cell diagram of Figure 6 are used for the layers numbered $2, 3, \ldots, N$ to indicate, respectively, their left and right positions with respect to the central layer. The central layer is marked $\tilde{1}$ to distinguish it from the layers on the other diagrams marked 1.

As a result, we may follow the method of [11], [12]. We begin with the solution in the central layer of the cell and expand it to the right and left layers using the continuity conditions of stress and displacement at the layer interfaces. Indeed, in a given layer of the cell, with constant material properties ρ and η and wave speed $c = \sqrt{\eta/\rho}$, the solution of (3) is of the form

$$u(x) = A \cos\left(\frac{\omega}{c} x\right) + B \sin\left(\frac{\omega}{c} x\right). \tag{17}$$

In the notation that follows $\rho_j^{\pm}$, $\eta_j^{\pm}$, and wave speed $c_j^{\pm} = \sqrt{\eta_j^{\pm}/\rho_j^{\pm}}$ indicate the corresponding values for the jth layer, $j = 2, \ldots, N$, located to the right ($(+)$ superscript) or left ($(-)$ superscript) of the central layer with $j = 1$.

As indicated in [11], [12], it is convenient to choose the two eigenfunctions $u_1(x)$ and $u_2(x)$ to be even and odd functions in the central layer,

$$u_1(x) = \cos\left(\frac{\omega}{c_1}x\right), \ -b_1 < x < d_1, \tag{18}$$

$$u_2(x) = \sin\left(\frac{\omega}{c_1}x\right), \ -b_1 < x < d_1. \tag{19}$$

The expansion of these solutions to the right and left layers would be of the form (17), and the eigenfunction $u_1(x)$ along the unit cell $[-b, d]$ can be given as

$$u_1(x) = \begin{cases} A_N^+ \cos\left(\frac{\omega}{c_N^+}(x - d_{N-1})\right) + B_N^+ \sin\left(\frac{\omega}{c_N^+}(x - d_{N-1})\right) & \text{for } d_{N-1} \le x \le d_N, \\ \vdots & \\ A_3^+ \cos\left(\frac{\omega}{c_3^+}(x - d_2)\right) + B_3^+ \sin\left(\frac{\omega}{c_3^+}(x - d_2)\right) & \text{for } d_2 \le x \le d_3, \\ A_2^+ \cos\left(\frac{\omega}{c_2^+}(x - d_1)\right) + B_2^+ \sin\left(\frac{\omega}{c_2^+}(x - d_1)\right) & \text{for } d_1 \le x \le d_2, \\ \cos\left(\frac{\omega}{c_1}x\right) & \text{for } -b_1 \le x \le d_1, \\ A_2^- \cos\left(\frac{\omega}{c_2^-}(x + b_1)\right) + B_2^- \sin\left(\frac{\omega}{c_2^-}(x + b_1)\right) & \text{for } -b_2 \le x \le -b_1, \\ A_3^- \cos\left(\frac{\omega}{c_3^-}(x + b_2)\right) + B_3^- \sin\left(\frac{\omega}{c_3^-}(x + b_2)\right) & \text{for } -b_3 \le x \le -b_2, \\ \vdots & \\ A_N^- \cos\left(\frac{\omega}{c_N^-}(x + b_{N-1})\right) + B_N^- \sin\left(\frac{\omega}{c_N^-}(x + b_{N-1})\right) & \text{for } -b_N \le x \le -b_{N-1}. \end{cases} \tag{20}$$

Using vector notation we denote

$$v_j^{\pm} = \begin{bmatrix} A_j^{\pm} \\ B_j^{\pm} \end{bmatrix}$$

for $j = 1, \ldots, N$.

The coefficients in (20), derived by the continuity conditions at the layer interfaces, are given by the recursive relations

$$v_{j+1}^{\pm} = M_j^{\pm} v_j^{\pm}, \tag{21}$$

where the matrix $M_j^{\pm}$ and the constant parameters are, respectively, given by

$$M_j^{\pm} = \begin{bmatrix} \cos\lambda_j^{\pm} & \pm\sin\lambda_j^{\pm} \\ \mp p_j^{\pm}\sin\lambda_j^{\pm} & p_j^{\pm}\cos\lambda_j^{\pm} \end{bmatrix} \tag{22}$$

and

$$\begin{cases} \lambda_j^+ = \frac{\omega}{c_j^+}(d_j - d_{j-1}), \ \lambda_j^- = \frac{\omega}{c_j^-}(b_j - b_{j-1}), \ p_j^{\pm} = \frac{\eta_j^{\pm} c_{j+1}^{\pm}}{\eta_{j+1}^{\pm} c_{j+1}^{\pm}}, \\ v_1^{\pm} = \begin{bmatrix} A_1^{\pm} \\ B_1^{\pm} \end{bmatrix} = \begin{bmatrix} 1 \\ 0 \end{bmatrix}, \ d_0 = 0, \ b_0 = 0 \end{cases} \tag{23}$$

for $j = 1, \ldots, N-1$. Here A_n^+ and B_n^+ are the coefficients of the eigenfunction $u_1(x)$ along the nth right layer, while A_n^-, B_n^- are the coefficients along the nth left layer. The layer interfaces are located at $-b = -b_N < -b_{N-1} < \cdots < -b_n < \cdots < -b_1 < d_1 < \cdots < d_n < \cdots < d_{N-1} < d_N = d$. Here $b_1 = d_1$, $b + d = a$ and $b_n > 0$, $d_n > 0$ for $n = 1, 2, \ldots, N$. Notice that the eigenfunction $u_1(x)$ is even in the central layer, but it does not necessarily remain even after it expands to the other layers of the cell; see Figure 7. The cell in Figure 7 is composed of five layers. Notice that at the layer interfaces, $u_1(x)$ develops corners, as expected from the stress continuity condition.

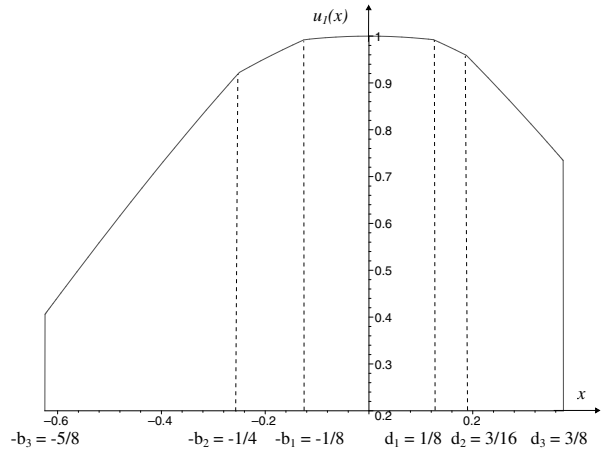

FIG. 7. *Eigenfunction $u_1(x)$ in a nonsymmetric cell of three materials and five layers. Additional parameters involved in* (20) *are $\omega = c_1 = c_2^{\pm} = c_3^{\pm} = 1$, $p_1^{\pm} = \frac{\eta_1}{\eta_2} = 4$, and $p_2^{\pm} = \frac{\eta_2}{\eta_3} = 2$.*

Similarly, we determine the eigenfunction $u_2(x)$ in the unit cell $[-b, d]$ as

$$u_2(x) = \begin{cases} A_N^{*+} \cos\left(\frac{\omega}{c_N^+}(x - d_{N-1})\right) + B_N^{*+} \sin\left(\frac{\omega}{c_N^+}(x - d_{N-1})\right) & \text{for } d_{N-1} \le x \le d_N, \\ \vdots & \\ A_3^{*+} \cos\left(\frac{\omega}{c_3^+}(x - d_2)\right) + B_3^{*+} \sin\left(\frac{\omega}{c_3^+}(x - d_2)\right) & \text{for } d_2 \le x \le d_3, \\ A_2^{*+} \cos\left(\frac{\omega}{c_2^+}(x - d_1)\right) + B_2^{*+} \sin\left(\frac{\omega}{c_2^+}(x - d_1)\right) & \text{for } d_1 \le x \le d_2, \\ \sin\left(\frac{\omega}{c_1} x\right) & \text{for } -b_1 \le x \le d_1, \\ A_2^{*-} \cos\left(\frac{\omega}{c_2^-}(x + b_1)\right) + B_2^{*-} \sin\left(\frac{\omega}{c_2^-}(x + b_1)\right) & \text{for } -b_2 \le x \le -b_1, \\ A_3^{*-} \cos\left(\frac{\omega}{c_3^-}(x + b_2)\right) + B_3^{*-} \sin\left(\frac{\omega}{c_3^-}(x + b_2)\right) & \text{for } -b_3 \le x \le -b_2, \\ \vdots & \\ A_N^- \cos\left(\frac{\omega}{c_N^-}(x + b_{M-1})\right) + B_N^- \sin\left(\frac{\omega}{c_N^-}(x + b_{N-1})\right) & \text{for } -b_N \le x \le -b_{N-1}. \end{cases} \tag{24}$$

Using vector notation we denote $v_j^{*\pm} = \begin{bmatrix} A_j^{*\pm} \\ B_j^{*\pm} \end{bmatrix}$ for $j = 1, \ldots, N$. The coefficients

of (24) are defined by the same recursive relations described in (21),

$$v_{j+1}^{*\pm} = M_j^{\pm} v_j^{*\pm}, \tag{25}$$

with

$$v_1^{*\pm} = \begin{bmatrix} A_1^{*\pm} \\ B_1^{*\pm} \end{bmatrix} = \begin{bmatrix} 0 \\ 1 \end{bmatrix}. \tag{26}$$

The matrix $M_j^{\pm}$ and the constant parameters d_0, b_0, $\lambda_j^{\pm}$, and $p_j^{\pm}$ for $j = 1, \ldots, N-1$ are given as before in (22)–(23).

Here A_n^{*+} and B_n^{*+} are the coefficients of the eigenfunction $u_2(x)$ along the nth right layer, while A_n^{*-}, B_n^{*-} are the coefficients along the nth left layer. Notice that $u_2(x)$ is odd in the central layer, but it does not necessarily remain odd after it expands to the other layers of the cell; see Figure 8. The cell in Figure 7 is composed of five layers. Notice that at the layer interfaces, $u_2(x)$ develops corners, as expected from the continuity of the stress condition.

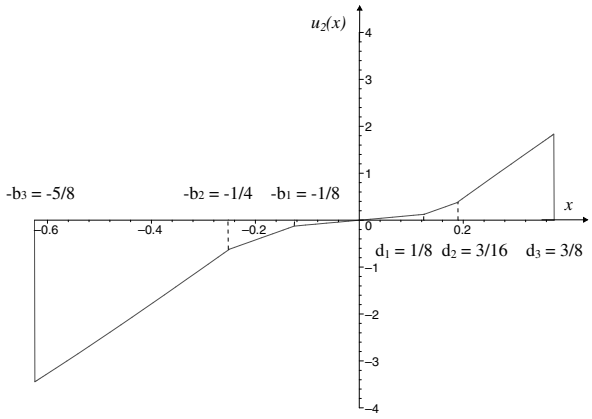

FIG. 8. *Eigenfunction $u_2(x)$ in a nonsymmetric cell of three materials and five layers. Additional parameters involved in* (24) *are $\omega = c_1 = c_2^{\pm} = c_3^{\pm} = 1$, $p_1^{\pm} = \frac{\eta_1}{\eta_2} = 4$, and $p_2^{\pm} = \frac{\eta_2}{\eta_3} = 2$.*

After evaluating $u_1(x)$ and $u_2(x)$ at the boundaries of the cell located at $x = -b$ and $x = d$, and then substituting these expressions into the general implicit formula of the dispersion relation (15), we obtain the following expressions for the numerator and the denominator, respectively:

$$\begin{aligned} &u_1(-b)u_2'(d) + u_1(d)u_2'(-b) - u_2(d)u_1'(-b) - u_2(-b)u_1'(d) \\ &= \frac{\omega}{c_N}(A_N^- B_N^{*+} + A_N^+ B_N^{*-} - A_N^{*+} B_N^- - A_N^{*-} B_N^+)\cos(\lambda_N^+ + \lambda_N^-) \\ &\quad + \frac{\omega}{c_N}(A_N^+ A_N^{*-} - B_N^{*+} B_N^- - A_N^{*+} A_N^{*-} + B_N^{*-} B_N^+)\sin(\lambda_N^+ + \lambda_N^-) \end{aligned} \tag{27}$$

and

$$u_1(-b)u_2'(-b) + u_2(-b)u_1'(-b) = \frac{\omega}{c_N}(A_N^- B_N^{*-} - A_N^{*-} B_N^-). \tag{28}$$

Recall that our leftmost layer is made of the same material as our rightmost layer, and hence $c_N^- = c_N^+ = c_N$.

Substituting (27) and (28) into the general implicit dispersion relation (15), we derive the *recursive formula for the dispersion relation*,

$$2\cos(qa) = \frac{(A_N^+ B_N^{*-} + A_N^- B_N^{*+} - A_N^{*+} B_N^- - A_N^{*-} B_N^+)\cos(\lambda_N^+ + \lambda_N^-)}{A_N^- B_N^{*-} - A_N^{*-} B_N^-} + \frac{(A_N^+ A_N^{*-} - A_N^- A_N^{*+} + B_N^+ B_N^{*-} - B_N^- B_N^{*+})\sin(\lambda_N^+ + \lambda_N^-)}{A_N^- B_N^{*-} - A_N^{*-} B_N^-}, \tag{29}$$

where the coefficients are obtained through the recursive relations involving (21)–(23), (25)–(26), while $\lambda_N^- = \frac{\omega}{c_N^-}(b_N - b_{N-1})$ and $\lambda_N^+ = \frac{\omega}{c_N^+}(d_N - d_{N-1})$. In the numerical experiments included in section 5, the recursive relation generating the coefficients $A_N^{\pm}, B_N^{\pm}, A_N^{*\pm}, B_N^{*\pm}$ of (29) is programmed in Maple [15]. The dispersion relation graph is then obtained using the *implicitplot* Maple command with the wave number q limited to the domain $0 \le q \le \pi/a$.

4. Recursive formula of the dispersion relation using the quasi-symmetric limiting approach. This alternative approach involves the quasi-symmetric cell configuration shown in Figure 9, which preserves the symmetric arrangement of the materials around the filler/central layer, and allows for layers of the same material to have differing lengths.

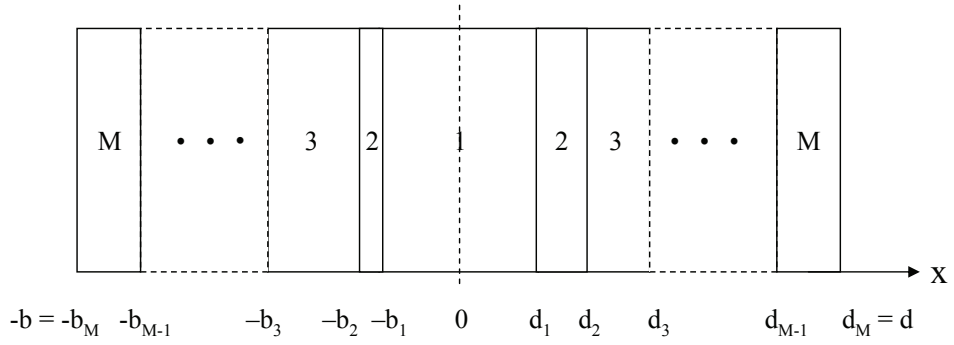

FIG. 9. *Quasi-symmetric configuration of a unit cell made of M materials.*

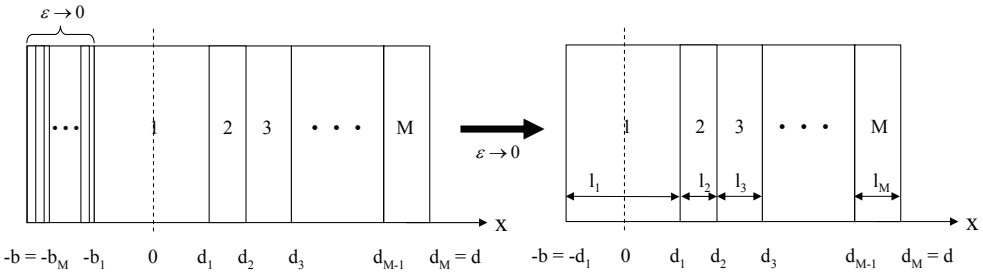

FIG. 10. *Obtaining the general cell configuration as a limiting case of the quasi-symmetric cell configuration.*

The quasi-symmetric limiting approach differs from the central expansion approach in the way the dispersion relation is derived for a general cell configuration with a non-quasi-symmetric configuration. The quasi-symmetric limiting approach views the general cell configuration as a limiting case of the quasi-symmetric configuration when the thickness of the left layer(s) approaches zero; see Figure 10. In the

limiting procedure, it is essential to start with a quasi-symmetric and nonsymmetric cell configuration. The same limiting procedure applied to a symmetric cell configuration would fail to produce any results, because in a symmetric cell configuration, as the thicknesses of the left layers approach zero, so do the thicknesses of the corresponding right layers. Thus, the quasi-symmetric nonsymmetric cell configuration is essential, as it allows the layer thicknesses to the left and right of the central layer to be arbitrary, and hence independent. This approach also highlights the fact that the dispersion formula obtained in [11], [12] works for a general symmetric cell configuration but fails once the cell configuration becomes quasi-symmetric. In summary, the quasi-symmetric configuration is a critical configuration to work with, because from there one can recover the dispersion relation for the general cell configuration, something that cannot be achieved from a symmetric configuration. The approach described above is summarized in Figure 11 and discussed in more detail below.

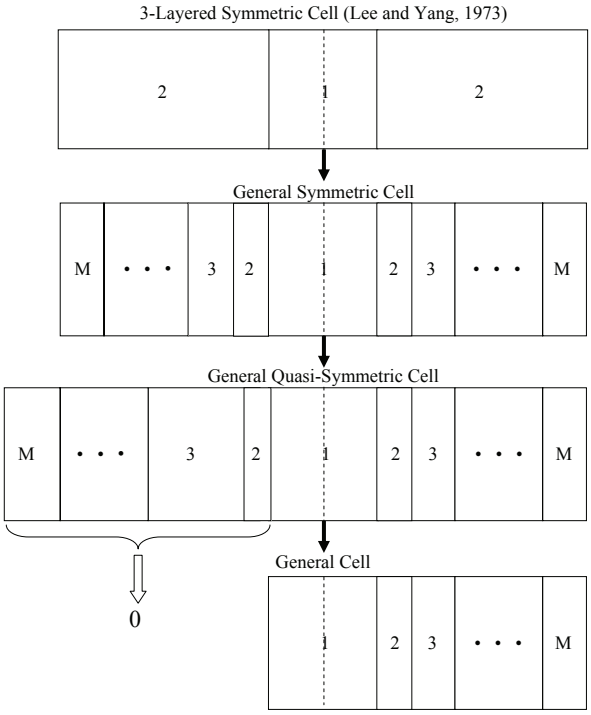

FIG. 11. *The stages of development of the quasi-symmetric limiting approach for a general cell configuration of M-layers.*

The recursive dispersion formula for the quasi-symmetric cell configuration can be derived similarly to that described in the previous section, under the simplifications that $\eta_j^- = \eta_j^+ = \eta_j$, $c_{j+1}^- = c_{j+1}^+ = c_{j+1}$, $p_j^- = p_j^+ = p_j$, and $N = M$ for $j = 1, 2, \ldots, M-1$. With these simplifications, the recursive dispersion formula (29) becomes

$$2\cos(qa) = \frac{(A_M^+ B_M^{*-} + A_M^- B_M^{*+} - A_M^{*+} B_M^- - A_M^{*-} B_M^+)\cos(\lambda_M^+ + \lambda_M^-)}{A_M^- B_M^{*-} - A_M^{*-} B_M^-} + \frac{(A_M^+ A_M^{*-} - A_M^- A_M^{*+} + B_M^+ B_M^{*-} - B_M^- B_M^{*+})\sin(\lambda_M^+ + \lambda_M^-)}{A_M^- B_M^{*-} - A_M^{*-} B_M^-}. \tag{30}$$

The coefficients are obtained through the recursive relations involving (21)–(23) and (25)–(26). Notice that $\lambda_M^- = \frac{\omega}{c_M}(b_M - b_{M-1})$, $\lambda_M^+ = \frac{\omega}{c_M}(d_M - d_{M-1})$, while $\lambda_j^- = \frac{\omega}{c_j}(b_j - b_{j-1})$, $\lambda_j^+ = \frac{\omega}{c_j}(d_j - d_{j-1})$, $p_j = \frac{\eta_j c_{j+1}}{\eta_{j+1} c_{j+1}}$ for $j = 1, \ldots, M-1$.

As for the general cell configuration, while the coefficients of (30) with (+) superscript corresponding to the right-hand side layers remain intact, the coefficients of the left-hand side layers with (−) superscript will simplify due to the fact that the left-hand side layers vanish; see Figure 10. From (21)–(23), it follows that the coefficients with (−) superscript related to the eigenfunction $u_1(x)$ along the left layers are given by

$$\begin{cases} A_{j+1}^- = A_j^- \cos(\lambda_j^-) - B_j^- \sin(\lambda_j^-), \\ B_{j+1}^- = p_j(B_j^- \cos(\lambda_j^-) + A_j^- \sin(\lambda_j^-)), \\ A_1^- = 1,\ B_1^- = 0,\ j = M-1, \ldots, 1. \end{cases} \tag{31}$$

In the limiting case, as $(b_j - b_{j-1})$ approaches zero, so does $\lambda_j = \frac{\omega}{c_j}(b_j - b_{j-1})$ for $j = M, \ldots, 2$. As a result, the recursive relation (31) becomes

$$\begin{cases} A_M^- = A_{M-1}^- = \cdots = A_j^- = \cdots = A_2^-, \\ B_M^- = p_{M-1} B_{M-1}^- = \cdots = p_{M-1} p_{M-2} \cdot p_j B_j^- = \cdots = p_{M-1} p_{M-2} \cdots p_2 B_2^-. \end{cases} \tag{32}$$

Furthermore, considering that $p_j = \frac{\eta_j c_{j+1}}{\eta_{j+1} c_j}$, $\lambda_1^+ = \lambda_1^- = \lambda_1$ (central layer), $A_1^- = 1$, and $B_1^- = 0$, the relations (32) become

$$\begin{cases} A_M^- = A_{M-1}^- = \cdots = A_j^- = \cdots = A_2^- = \cos(\lambda_1), \\ B_M^- = \dfrac{\eta_{M-1} c_M}{\eta_M c_{M-1}} B_{M-1}^- = \cdots = \dfrac{\eta_j c_M}{\eta_M c_j} B_j^- = \cdots = \dfrac{\eta_2 c_M}{\eta_M c_2} B_2^- = \dfrac{\eta_1 c_M}{\eta_M c_1} \sin(\lambda_1). \end{cases} \tag{33}$$

As a result, the coefficients A_M^-, B_M^-, and similarly A_M^{*-} and B_M^{*-}, simplify to

$$A_M^- = \cos(\lambda_1) \quad \text{and} \quad B_M^- = \frac{\eta_1 c_M}{\eta_M c_1} \sin(\lambda_1), \tag{34}$$

$$A_M^{*-} = -\sin(\lambda_1) \quad \text{and} \quad B_M^{*-} = \frac{\eta_1 c_M}{\eta_M c_1} \cos(\lambda_1). \tag{35}$$

The parameters to be used in numerical experiments (see Figure 10 and Figure 14) are

$$d_0 = 0, \quad d_1 = l_1/2, \quad d_j = l_1/2 + \sum_{h=2}^{j} l_h, \quad b_0 = 0, \quad b_j = l_1/2, \quad j = 1, 2, \ldots, M,$$

that is,

$$\lambda_1^+ = \lambda_1^- = \lambda_1 = \frac{\omega l_1}{2c_1}, \quad \lambda_j^+ = \lambda_j = \frac{\omega l_j}{c_j}, \quad \lambda_j^- = 0, \quad j = 1, 2, \ldots, M.$$

Finally, by substituting (34) and (35) in the recursive dispersion relation (30) for the quasi-symmetric configuration, we obtain the recursive dispersion relation (36) for the general configuration of the unit cell made of M layers/materials.

(36)

$$\begin{aligned} 2\cos(qa) = \tfrac{c_1 \eta_M}{c_M \eta_1} [&(A_M^+ \tfrac{\eta_1 c_M}{\eta_M c_1} \cos\lambda_1 + \cos\lambda_1 B_M^{*+} - A_M^{*+} \tfrac{\eta_1 c_M}{\eta_M c_1} \sin\lambda_1 + \sin\lambda_1 B_M^+) \cos(\lambda_M) \\ &+ (-A_M^+ \sin\lambda_1 - \cos\lambda_1 A_M^{*+} + B_M^+ \tfrac{\eta_1 c_M}{\eta_M c_1} \cos\lambda_1 - B_M^{*+} \tfrac{\eta_1 c_M}{\eta_M c_1} \sin\lambda_1) \sin(\lambda_M)]. \end{aligned}$$

Here the coefficients with a (+) superscript are generated using the recursive relations (21)–(23) and (25)–(26). In summary, we established in (36) a recursive dispersion relation for the general configuration of the unit cell made of M layers/materials. This formula was obtained by considering the quasi-symmetric cell configuration as an essential intermediate step. For cell configurations that are already quasi-symmetric or symmetric, the recursive dispersion relation expressed by (30) is more suitable, as it involves fewer recursive steps.

5. Numerical results: Comparison of the central expansion approach with the method by Shen and Cao given in [18].

5.1. Three-material cell ($M = 3$). We consider a cell composed of three distinct materials: concrete, nickel alloy, and steel. The lengths of the layers are 0.2 m, 0.25 m, and 0.3 m, respectively. The general cell diagram in Figure 6 illustrates the unit cell used in [18] for $M = 3$. In the central expansion approach, a shifting and renumbering of the layers in the original cell takes place. The resulting cell is illustrated by the renumbered cell diagram given in Figure 6 with $N = \lceil \frac{M}{2} \rceil + 1 = \lceil \frac{3}{2} \rceil + 1 = 3$, hence the need for a fake interface. As a result, the cell to be used with the central expansion approach has five layers and the materials for each layer are steel, nickel, concrete, concrete, and steel. Notice the introduction of a fake interface on the original layer of concrete. The material parameters (elastic modulus and density) are given in the appendix.

The two graphs of the dispersion relation obtained using the central expansion approach given in (29), and Shen and Cao's formulas in [18], overlap in Figure 12, demonstrating the consistency between the two methods. The recursive relation generating the coefficients $A_N^{\pm}, B_N^{\pm}, A_N^{*\pm}, B_N^{*\pm}$ of (29) is programmed in Maple [15]. The dispersion relation graph is then obtained using the *implicitplot* Maple command. Determining more accurately the values of the circular frequency ω for a given value of q, including the band ends with $qa = 0$ or $qa = \pi$, is a difficult root-finding problem. As discussed in [11], [12], due to (4), it is only necessary to consider the wave number q limited to the domain $0 \leq q \leq \pi/a$. As seen in Figure 12, the dispersion relation graph displays a banded frequency spectrum using the reduced zone scheme for the wave number q, with the circular frequency ω in the ordinate. The banded frequency spectrum is composed of pass or propagating bands and stop bands. Over the interval $0 \leq q \leq \pi/a$, bands of permissible frequencies appear, separated by forbidden bands (creating bandgaps), at which frequencies no Floquet waves can be propagated. This band structure of pass and nonpass bands shows the dispersive properties of the medium. Similar comments can be made for the other dispersion relation graphs.

5.2. Four-material cell ($M = 4$). Similarly, we consider a cell composed of four distinct materials: steel, aluminum, concrete, and nickel alloy. The lengths of the layers are 0.15 m, 0.1 m, 0.4 m, and 0.2 m, respectively. As before, the general cell diagram in Figure 6 illustrates the unit cell used in [18], when $M = 4$. The cell used for the central expansion approach is illustrated by the renumbered cell diagram given in Figure 6 with $N = \lceil \frac{M}{2} \rceil + 1 = \lceil \frac{4}{2} \rceil + 1 = 3$. Notice that unlike the three-material case, in this case we do not need to add a fake interface because the number of layers after the shift is already odd. The materials for each of the five layers are nickel alloy, steel, aluminum, concrete, and nickel alloy. We plot the dispersion relation using both methods, as shown in Figure 13. Notice again how well the two graphs overlap.

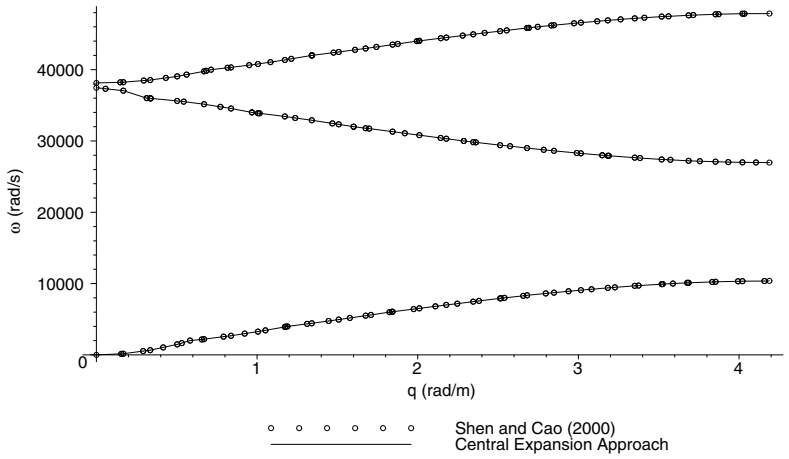

FIG. 12. *Dispersion graphs for a three-material cell: Central expansion approach versus Shen and Cao* [18]*, using the reduced zone scheme for the wave number* q*.*

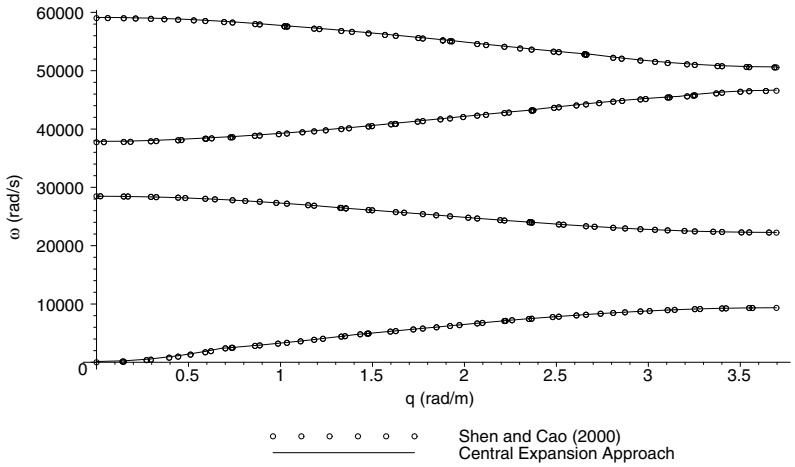

FIG. 13. *Dispersion graphs for a four-material cell: Central expansion approach versus Shen and Cao* [18]*, using the reduced zone scheme for the wave number* q*.*

6. Numerical results: Quasi-symmetric limiting approach.

6.1. Comparison of the quasi-symmetric limiting approach with the method by Shen and Cao in [18]. Here we consider a unit cell composed of five layers arranged in a general configuration, shown in Figure 14. We choose aluminum as material 1, nickel alloy as material 2, concrete as materials 3 and 5, and steel as material 4, with the following layer thicknesses: $l_1 = 0.1$ m, $l_2 = 0.05$ m, $l_3 = 0.4$ m, $l_4 = 0.2$ m, and $l_5 = 0.25$ m. The material parameters (elastic modulus and density) can be found in the appendix. The two graphs displaying the dispersion relation using the quasi-symmetric limiting approach given in (36), and Shen and Cao's formulas in [18], overlap in Figure 15.

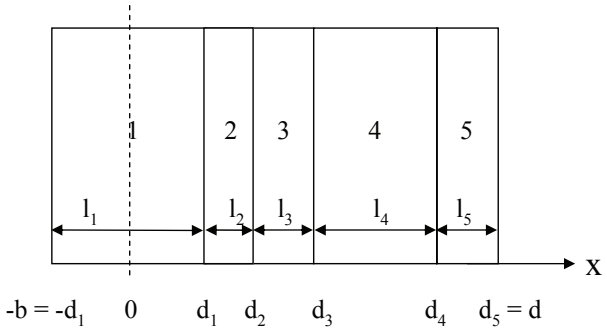

FIG. 14. *General configuration of a five-layer cell.*

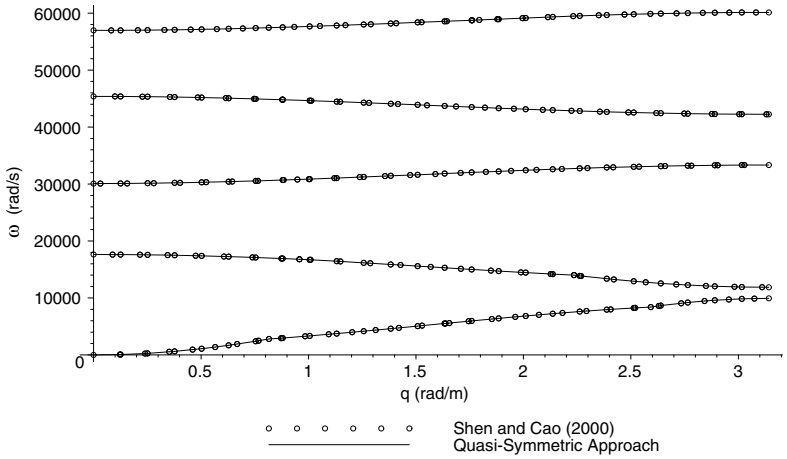

FIG. 15. *Dispersion graphs for a five-layer cell: Quasi-symmetric limiting approach versus Shen and Cao* [18]*, using the reduced zone scheme for the wave number q.*

6.2. Comparison of both of our approaches with experimental results: A simplified one-dimensional model. The dispersion relation and sound attenuation through three-dimensional structures composed of periodically arranged cubic cells were experimentally measured in [13]. The cubic single cell consisted of a 1 cm diameter spherical core made of lead, coated with a 2.5 mm layer of silicone rubber. The coated spheres were periodically arranged in a $8 \times 8 \times 8$ cubic crystal with lattice constant of 1.55 cm, and with epoxy as the surrounding matrix material. The cross section of the cell is displayed on the upper part of Figure 16. The one-dimensional, three-material symmetric cell model, shown in the lower part of Figure 16, may be viewed, as suggested by Wang et al. [23], as a simplified one-dimensional counterpart of the three-dimensional structure studied in [13]. In our one-dimensional model, lead is considered as material 1, silicone rubber as material 2, and epoxy as material 3 with the following layer lengths: 1 cm (central), with 0.25 cm and 0.025 cm on each side. The material parameters (elastic modulus and density) are included in the appendix. Our intent here is to illustrate the fact that our dispersion relations correctly predict bandgaps due to a so-called localized resonance phenomenon that has been observed in three-dimensional ternary systems [13]; the localized resonance

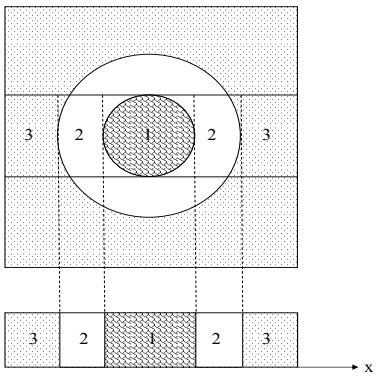

FIG. 16. *One-dimensional unit cell motivated from the three-dimensional cubic structure (cross section) studied in* [13].

can reduce the magnitude of the bandgap by two orders of magnitude relative to that caused by Bragg scattering, and this observation has spurred renewed interest by the acoustic bandgap community for design of acoustic attenuators. In [6], Bragg's law $f = n * v/2a$, for example, predicts a scattering frequency of about 62.5 KHz using steel scatterers embedded in an epoxy matrix with a lattice constant of 20 mm. Here, v is the longitudinal wave speed of the matrix, and a is the distance between the centers of the scatterers ($n = 1, 2, 3, \ldots$).

Liu et al. [13] measured acoustic transmission T as a function of frequency (250 Hz to 1600 Hz) by placing a receiving transducer at the center of their sonic crystals with an external sound source. The lowest values of T correspond to wave frequencies that are attenuated by the structure, whereas the highest values of T correspond to wave frequencies that easily propagate throughout the structure. Their experiments reveal that peak transmission frequencies are located at $f = 600$ Hz and $f = 1600$ Hz. Between these two frequencies, the transmission coefficient is low. The few measurements made for low frequency ($f \simeq 300$ Hz) suggest that waves with low frequencies easily propagate through the structure.

Due to the symmetric cell configuration of the one-dimensional simplified model given in Figure 16, the central expansion approach and the quasi-symmetric limiting approach share the same dispersion relation formula (29). The graph in Figure 17 displays the dispersion relation predicted by (29) and obtained using the *implicitplot* Maple command. Here we use frequency f on the ordinate instead of the circular frequency ω. Determining more accurately the values of the frequency f for a given value of q, including the band ends with $qa = 0$ or $qa = \pi$, is a difficult root-finding problem. As seen in Figure 17, between the frequency range of 0–2000 Hz, the graph exhibits a pass band for low frequencies under 140 Hz, and what appear to be four additional narrow pass bands centered approximately at $f = 873$, $f = 950$, $f = 1353$, and $f = 1907$ Hz. Closer inspection of an expanded view of the second pass band shows that it is centered at $f = 873.5$ Hz (Figure 18). Expanded views of the third and fourth bands (not shown here) located at approximately 950 Hz and 1353 Hz are essentially flat to within numerical roundoff, hence the group velocity at these frequencies is zero, i.e., $v_g = \frac{df}{dq} = 0$.

In conclusion, our one-dimensional model appears to qualitatively predict the acoustic response of the three-dimensional ternary structure, with the two narrow pass

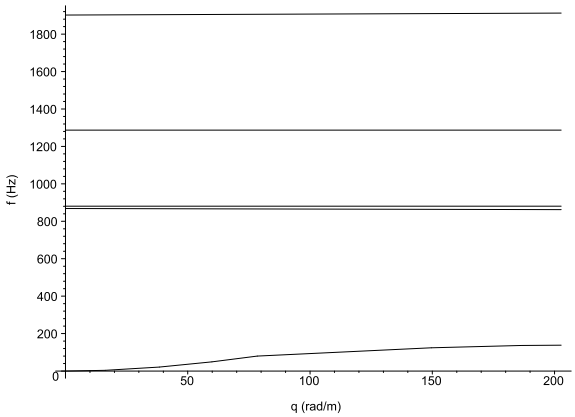

FIG. 17. *Graph of the dispersion relation for one-dimensional symmetrical cell model motivated from the three-dimensional model of* [13]*, using the reduced zone scheme for the wave number* q*.*

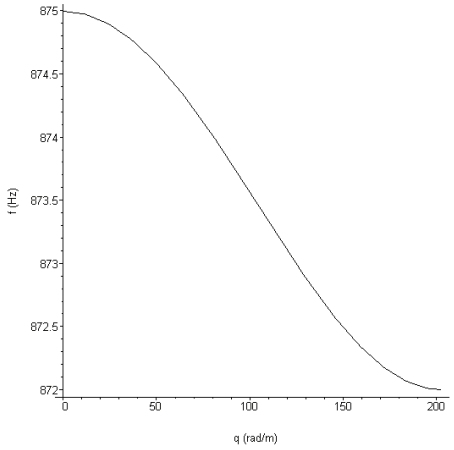

FIG. 18. *Expanded view of the second pass band illustrated in Figure* 17*.*

bands corresponding to the peaks and the two large bandgaps corresponding to the ranges of frequencies that are highly attenuated. Our numerical simulations predict bandgaps with a lattice constant two orders of magnitude smaller than the relevant wavelength, suggesting a so-called localized resonance phenomenon already observed in three-dimensional ternary systems [13]. However, the locations of the bandgaps do not match those that are experimentally observed. This is to be expected, considering the fact that our band structure equations are derived for infinite one-dimensional periodic elastic media whereas the experiments in [13] were conducted on a finite three-dimensional structure, with bandgaps only partially developed.

Appendix. The following are the elastic modulus η and density ρ of the materials selected for the numerical experiments:

1. Concrete: $\eta = 33 \cdot 10^9$ Pa and $\rho = 2400$ kg/m^3.
2. Steel: $\eta = 210 \cdot 10^9$ Pa and $\rho = 7800$ kg/m^3.
3. Aluminum: $\eta = 69 \cdot 10^9$ Pa and $\rho = 2710$ kg/m^3.

4. Nickel Alloy: $\eta = 214 \cdot 10^9$ Pa and $\rho = 8130$ kg/m^3.
5. Lead: $\eta = 40.8 \cdot 10^9$ Pa and $\rho = 11600$ kg/m^3.
6. Silicone rubber: $\eta = 117500$ Pa and $\rho = 1300$ kg/m^3.
7. Epoxy: $\eta = 4.4 \cdot 10^9$ Pa and $\rho = 1180$ kg/m^3.

Acknowledgment. The authors would like to acknowledge the two reviewers of this paper for their valuable suggestions and constructive comments.

REFERENCES

[1] A. Ben-Menahem and S. J. Singh, *Seismic Waves and Sources*, Springer-Verlag, New York, 1981.
[2] L. Brillouin, *Wave Propagation in Periodic Structures*, Dover, New York, 1946.
[3] W. Cao and W. Qi, *Plane wave propagation in finite 2-2 composites*, J. Appl. Phys., 78 (1995), pp. 4627–4632.
[4] P. Goupillaud, *An approach to inverse filtering of near-surface layer effects from seismic records*, Geophys., 26 (1961), pp. 754–760.
[5] N. A. Haskell, *The dispersion of surface waves on multilayered media*, Bull. Seismol. Soc. Amer., 43 (1953), pp. 17–34.
[6] M. Hirsekorn, P. P. Delsanto, N. K. Batra, and P. Matic, *Modelling and simulation of acoustic wave propagation in locally resonant sonic materials*, Ultrasonics, 42 (2004), pp. 231–235.
[7] M. I. Hussein, G. M. Hulbert, and R. A. Scott, *Dispersive elastodynamics of 1D banded materials and structures: Analysis*, J. Sound Vibration, 289 (2006), pp. 779–806.
[8] M. I. Hussein, G. M. Hulbert, R. A. Scott, and K. Saitou, *Multiobjective evolutionary optimization of periodic layered materials for desired wave dispersion characteristics*, Struct. Multidiscip. Optim., 31 (2006), pp. 60–75.
[9] E. R. Kanasewich, *Time Sequence Analysis in Geophysics*, University of Alberta Press, Edmonton, Alberta, 1973.
[10] M. S. Kushwaha, *Classical band structure of periodic elastic composites*, Internat. J. Modern Phys. B, 10 (1996), pp. 977–1094.
[11] E. H. Lee, *A survey of variational methods for elastic wave propagation analysis in composites with periodic structures*, in Dynamics of Composite Materials, E. H. Lee, ed., ASME, New York, 1972, pp. 122–138.
[12] E. H. Lee and W. H. Yang, *On waves in composite materials with periodic structure*, SIAM J. Appl. Math., 25 (1973), pp. 492–499.
[13] Z. Liu, X. Zhang, Y. Mao, Y. Y. Zhu, Z. Yang, C. T. Chan, and P. Sheng, *Locally resonant sonic materials*, Science, 289 (2000), pp. 1734–1736.
[14] W. Magnus and S. Winkler, *Hill's Equation*, John Wiley, New York, 1996.
[15] *Maple* 12 *User Manual*, Waterloo Maple, Waterloo, ON, Canada, 2008.
[16] W. L. Pilant, *Elastic Waves in the Earth*, Elsevier Science, New York, 1979.
[17] Lord Rayleigh, *On the maintenance of vibrations of forces of double frequency, and on the propagation of waves through a medium endowed with a periodic structure*, Phil. Mag., 24 (1887), pp. 145–159.
[18] M. Shen and W. Cao, *Acoustic bandgap formation in a periodic structure with multilayer unit cells*, J. Phys. D, 33 (2000), pp. 1150–1154.
[19] J. W. C. Sherwood and A. W. Trorey, *Minimum-phase and related properties of the response of horizontally stratified absorptive earth to plane acoustic waves*, Geophys., 30 (1965), pp. 191–197.
[20] C. T. Sun, J. D. Achenbach, and G. Herrmann, *Continuum theory for a laminated medium*, J. Appl. Mech., 35 (1968), pp. 467–475.
[21] W. T. Thomson, *Transmission of elastic waves through a stratified solid medium*, J. Appl. Phys., 21 (1950), pp. 89–93.
[22] S. Treitel and E. A. Robinson, *Seismic wave propagation in layered media in terms of communication theory*, Geophys., 31 (1966), pp. 17–32.
[23] G. Wang, D. Yu, J. Wen, Y. Liu, and X. Wen, *One-dimensional phononic crystals with locally resonant structures*, Phys. Lett. A, 327 (2004), pp. 512–521.
[24] S. Yang, J. H. Page, Z. Liu, M. L. Cowan, C. T. Chan, and P. Sheng, *Ultrasound tunneling through 3D phononic crystals*, Phys. Rev. Lett., 88 (2002), article 104301.